Journal of Catalysis **207,** 202–212 (2002)
doi:10.1006/jcat.2002.3519, available online at http://www.idealibrary.com on IDEAL®

Kinetics of the CO + NO Reaction over Bimetallic Platinum–Rhodium on Alumina: Effect of Ceria Incorporation into Noble Metals

P. Granger,*,[1] L. Delannoy,* J. J. Lecomte,* C. Dathy,* H. Praliaud,† L. Leclercq,* and G. Leclercq*

*Université des Sciences et Technologies de Lille, Laboratoire de Catalyse, UPRESA 8010, Bât. C3, 59650-Villeneuve d'Ascq Cédex, France; and †Laboratoire d'Application de la Chimie à l'Environnement, UMR 9977, Université Claude Bernard Lyon I, 69622-Villeurbanne Cedex, France

Received June 15, 2001; revised January 4, 2002; accepted January 4, 2002

The influence of ceria on the kinetic behavior of noble metals in the reduction of NO by CO has been investigated at 120 and 300°C on a freshly prepared Pt–Rh/Al_2O_3–CeO_2 catalyst, and on an aged catalyst after reaction for 16 h at 500°C, within pressure ranges of 2.3–9 × 10^{-3} atm for CO and 1.5–8 × 10^{-3} atm for NO, using a differential fixed-bed flow reactor. These two temperatures have been selected from temperature-programmed experiments because they correspond to two very different regimes of activity of noble metals with ceria. It has been found that a rate equation derived from a bifunctional mechanism involving reaction paths either on metal or on ceria can correctly fit rate measurements performed at 120°C. In contrast a conventional mechanism earlier proposed for modeling the CO + NO reaction on Pt–Rh/Al_2O_3 at 300°C, where only noble metals are involved, enables modeling of rate measurements at 300°C on Pt–Rh/Al_2O_3–CeO_2, which suggests that the interaction between ceria and noble metals is suppressed at that temperature. The temperature dependency of the rate constants and equilibrium constants for NO and CO adsorption has been quantified in order to explain such changes in the kinetic behavior of Pt–Rh/Al_2O_3–CeO_2.

1. INTRODUCTION

The reduction of CO, NO, and hydrocarbon emissions from automotive exhaust gases has been extensively studied in the past two decades (1, 2). Presently the three-way catalyst technology is adopted all over the world and reduces efficiently NO_x emissions in a wide range of air-to-fuel ratios. The typical active components of three-way catalysts (TWCs) are noble metals with various additives, such as ceria and zirconia (3, 4), which improve their oxygen storage capacity. However after aging of the catalyst, a loss of oxygen storage capacity is observed (5). Moreover, the more severe restrictions on NO_x emissions set by the legislation need more-efficient TWCs, which implies a better understanding of the nature of the interaction between ceria and noble metals. It has also been shown that the presence of ceria increases thermal stability and noble metal dispersion (6, 7) and promotes the water–gas shift reaction (8). The extent of interaction between ceria and noble metals can induce considerable changes in the reactivity of intermediates and their adsorptive properties over noble metals (9, 10). Presently, the clarification of the mechanisms at atomic scale as well as the establishment of reliable kinetic models (11) are of prime importance for attempts to optimize the interaction between ceria and the noble metals.

Earlier investigations into the kinetics of the CO + NO reaction over Pt- and Rh-based catalysts, performed in our laboratory, led to the selection of the following mechanism involving the dissociation of NO via step [3], which has been assumed to be rate limiting (12, 13).

$$CO + * \Leftrightarrow CO_{ads}, \quad [1]$$

$$NO + * \Leftrightarrow NO_{ads}, \quad [2]$$

$$NO_{ads} + * \rightarrow N_{ads} + O_{ads}, \quad [3]$$

$$NO_{ads} + N_{ads} \rightarrow N_2O + 2^*, \quad [4]$$

$$NO_{ads} + N_{ads} \rightarrow N_2 + O_{ads} + *, \quad [5]$$

$$N_{ads} + N_{ads} \rightarrow N_2 + 2^*, \quad [6]$$

$$CO_{ads} + O_{ads} \rightarrow CO_2 + 2^*, \quad [7]$$

where $*$ stands for a vacant adsorption site.

Contrary to what has been observed on Pt/Al_2O_3, step [6] can be neglected on Rh-based catalysts (13) but not Pt. It was shown that Eq. [8], based on noncompetitive adsorptions of NO and CO, respectively, on Rh and Pt sites and a surface predominantly populated by adsorbed NO and CO molecules, correctly fits the influence of the partial pressures on the rate of NO transformation on Pt–Rh/Al_2O_3 (13). This equation also accounts for the fact that the nearest-neighbor adsorption site, involved in NO dissociation (step [3]), is mainly composed of Pt.

$$r_{NO} = \frac{2k_3\lambda_{NO}P_{NO}}{(1 + \lambda_{NO}P_{NO})\,(1 + \lambda_{CO}P_{CO})}, \quad [8]$$

where k_3 is the rate constant of the dissociation of NO

[1] To whom correspondence should be addressed. Fax: +33 3 20 33 61 21. E-mail: Pascal.Granger@univ-lille1.fr.

0021-9517/02 $35.00

according to step [3], and λ_i and P_i are, respectively, the equilibrium adsorption constants and the partial pressures of the reactants (i = CO or NO).

This third paper of the series has been devoted to the study of the effect of ceria addition on the catalytic behavior of noble metals in Pt–Rh/Al_2O_3–CeO_2. Particular attention has been paid to the synergy effect on the catalytic performances earlier observed in the CO + NO reaction (14, 15), which is generally explained by the involvement of interactions between noble metals and oxygen vacancies (16–18). Oh (9) suggests that the high rates for the dissociation of NO (step [3]), and the desorption of N_2 (step [6]), could explain changes in the kinetics of the CO + NO reaction when ceria interacts with Rh. Alternately, such a beneficial effect can be explained from a different mechanism involving anionic vacancies as active sites for the dissociation of NO (3, 4, 19).

This study deals with the kinetics of the CO + NO reaction on Pt–Rh/Al_2O_3–CeO_2. We first checked to see if Eq. [8] is still valid for modeling the partial pressure dependency of the reaction rate, or if it implies a rate equation derived from a bifunctional mechanism involving the redox properties of ceria. The comparison of the values of k_3, λ_{NO}, and λ_{CO}, with those previously estimated on Pt–Rh/Al_2O_3, with additional spectroscopic observations allows discussion of the effective role of ceria in modifying the properties of noble metals, and their subsequent catalytic performances.

2. EXPERIMENTAL

2.1. Catalysts

The catalyst preparation was described in Ref. (15). Al_2O_3–12 wt% CeO_2 was synthesized by impregnation of γ-Al_2O_3 with a solution of cerium nitrate. After water evaporation, the solid thus obtained was dried overnight at 120°C, then calcined in air at 550°C. X-ray diffraction (XRD) analysis did not reveal bulk detectable cerium oxide species. Pt–Rh/Al_2O_3–CeO_2 was prepared according to the conventional coimpregnation procedure. The impregnated sample was successively calcined in air at 350°C and reduced in pure H_2 at 450°C for 2 h. Such a procedure was also applied to the preparation of the reference Pt–Rh/Al_2O_3 catalyst (13).

2.2. Kinetic Experiments

The CO + NO reaction was studied in a fixed-bed flow reactor earlier described (13). Differential conditions were achieved by recycling the outlet gas mixture with a high recycling ratio, of about 180, in order to minimize external heat and mass transfer restrictions. The catalyst was in a powder form with an average particle size of 80 μm. The feedstream composition was analyzed by means of a Hewlett Packard 5890 series II chromatograph fitted with a thermal conductivity detector. Products and reactants were separated on a CTR1 column from Alltech. Prior to reaction, the catalyst was initially *in situ* reduced in H_2, outgassed in flowing helium at 400°C, and finally cooled at room temperature (RT). Steady state rate measurements at 300°C were performed on a reduced Pt–Rh/Al_2O_3–CeO_2 further heated in the reacting mixture at 500°C for 16 h. The experimental conditions used for the reaction were a total flow rate of 10 L h^{-1} with 0.05–0.2 g of catalyst mixed with 0.2–0.8 g of α-Al_2O_3, corresponding to space velocities in the range 25,000–120,000 h^{-1}.

The formation of N_2 and N_2O was only observed from the reduction of NO, according to the following reactions:

$$2NO + 2CO \rightarrow N_2 + 2CO_2, \quad [9]$$

$$2NO + CO \rightarrow N_2O + CO_2. \quad [10]$$

The overall conversions of NO (τ_{NO}) and of CO (τ_{CO}), related to the reduction of NO, are given by Eqs. [11] and [12], where τ_{N_2} and τ_{N_2O} are, respectively, the conversion of NO into N_2 and N_2O. n_i^0 is the inlet amount of the reactants while n_{N_2} and n_{N_2O} are, respectively, the amount of N_2 and N_2O produced at any time. P_i^0 is the inlet partial pressure of the reactant i.

$$\tau_{NO} = \frac{2\left(n_{N_2} + n_{N_2O}\right)}{n_{NO}^0} = \tau_{N_2} + \tau_{N_2O}, \quad [11]$$

$$\tau_{CO} = \frac{2\,n_{N_2} + n_{N_2O}}{n_{CO}^0} = \left(\tau_{N_2} + \frac{\tau_{N_2O}}{2}\right)\frac{n_{NO}^0}{n_{CO}^0} = \left(\tau_{N_2} + \frac{\tau_{N_2O}}{2}\right)\frac{P_{NO}^0}{P_{CO}^0}. \quad [12]$$

2.3. Spectroscopic Measurements

2.3.1. X-ray photoelectron spectroscopy (XPS). XPS measurements were performed with a Leybold Heraeus LHS10 spectrometer equipped with a magnesium anode ($h\nu$ = 1253.6 eV). Before analysis under ultrahigh vacuum (UHV) conditions, the catalyst samples were preheated *in situ* in 10 vol% H_2 diluted in helium at 425°C, then transferred to the analysis chamber. The binding energies (B.E.) were referenced to the Al 2p level (74.6 eV). The accuracy on the B.E. values was ±0.3 eV.

2.3.2. Infrared spectroscopy. Fourier transform infrared (FTIR) spectra were recorded on a Brucker Vector 22 spectrometer, under controlled atmosphere, at room temperature. Prior to analysis, the samples were reduced *in situ* in flowing hydrogen at 500°C, then outgassed under vacuum at 350°C for 1 h. Finally the cell was cooled at RT before admitting 1.3×10^{-2} atm of CO. The catalyst samples were maintained in these operating conditions for 1 h; finally CO was evacuated.

3. RESULTS

3.1. Kinetic Measurements

3.1.1. Preliminary temperature-programmed CO + NO reaction (TPR). Temperature-programmed experiments of the CO + NO reaction on a freshly prepared Pt–Rh/Al_2O_3–CeO_2 were performed from room temperature to 500°C in stoichiometric conditions with an inlet partial pressure for NO and CO of 5×10^{-3} atm. Immediately after admission of the reactant mixture at RT, a significant NO conversion was observed without subsequent CO conversion, which has been assigned to surface reoxidation of Ce^{3+} formed by Ce^{4+} reduction during the reductive pretreatment in H_2 (20). As shown in Fig. 1, the CO + NO reaction starts on Pt–Rh/Al_2O_3–CeO_2 below 50°C (first run) instead of ~150°C for the less-active Pt–Rh/Al_2O_3. It is intriguing that the low-temperature conversion range on the ceria-promoted catalyst stabilizes from 200°C, while it should rise monotonically with the temperature. This observation could be related to the concomitant suppression of the synergy effect of ceria on the activity of noble metals or/and to the occurrence of deactivation phenomena. Above 280°C, the conversion curves of both catalysts are superimposed, which suggests that the mechanism describe on Pt–Rh/Al_2O_3 probably dominates on Pt–Rh/Al_2O_3–CeO_2. The reaction was continued on Pt–Rh/Al_2O_3–CeO_2 at 500°C for 72 h; finally the catalyst was cooled at room temperature in the reactant mixture. A second run was performed on the aged Pt–Rh/Al_2O_3–CeO_2. The low-temperature conversion range is still observable, which suggests reversible changes in the kinetics of the CO + NO reaction, with the synergy effect being limited to the low-temperature range (below 280°C). However a strong attenuation is also observed for this low-temperature conversion range, which probably indicates deactivation phenomena.

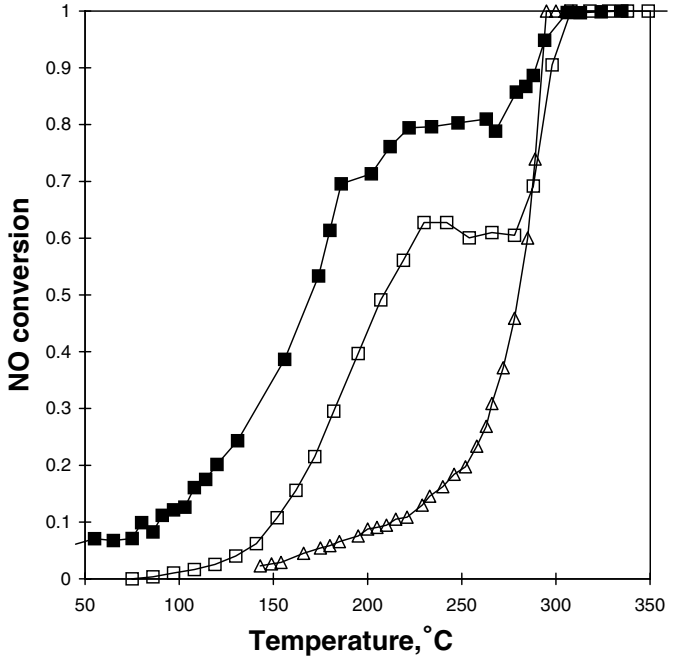

FIG. 1. Temperature-programmed conversion curves for the CO + NO reaction on Pt–Rh/Al_2O_3 (△) and on Pt–Rh/Al_2O_3–CeO_2 (■, first run); (□) second run after 72-h aging in the course of the reaction at 500°C, with $P_{NO} = P_{CO} = 5 \times 10^{-3}$ atm, $m_{CAT} = 0.2$ g, and total flow rate = 10 L h^{-1}.

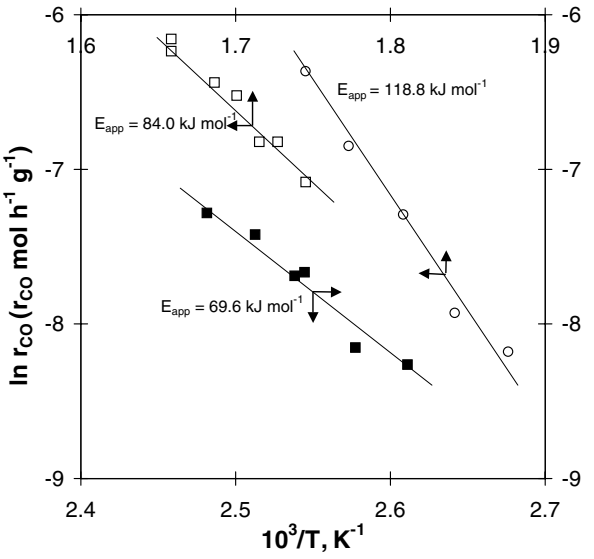

FIG. 2. Arrhénius plots for the CO + NO reaction on Pt–Rh/Al_2O_3 (○) and on Pt–Rh/Al_2O_3–CeO_2 in the range 110–120°C (■) and 300–330°C (□), with $P_{NO} = P_{CO} = 5 \times 10^{-3}$ atm, $m_{CAT} = 0.2$ g, and total flow rate = 10 L h^{-1}.

3.1.2. Steady state kinetic measurements. Steady state kinetic measurements were performed below 140°C, corresponding to the low-temperature conversion range, on a freshly prepared Pt–Rh/Al_2O_3–CeO_2 catalyst *in situ* reduced in hydrogen at 500°C, and above 280°C when the synergy effect of ceria attenuates.

Effect of temperature. Rate measurements were performed in stoichiometric conditions with inlet NO and CO partial pressures of 5×10^{-3} atm in the temperature range 110–120°C and 300–330°C. The apparent activation energies for the CO oxidation by NO corresponding to these two ranges of temperature have been estimated from the slope of the Arrhénius plots shown in Fig. 2. The values obtained on Pt–Rh/Al_2O_3–CeO_2 are, respectively, 69.6 and 84.0 kJ mol^{-1}. The corresponding value previously estimated on Pt–Rh/Al_2O_3, ~119 kJ mol^{-1}, emphasizes earlier observations related to a decrease in the apparent activation energy after ceria addition to noble metals (9, 16, 21, 22).

Influence of the reactant partial pressures on the rate of CO transformation. The influence of CO and NO partial pressures has been investigated at 120 and 300°C, respectively,

TABLE 1

Effect of Temperature and Partial Pressures of the Reactants on the Rate of the CO + NO Reaction on Pt–Rh/Al_2O_3–CeO_2

Temp.	P_{NO} (10^{-3} atm)	P_{CO} (10^{-3} atm)	r_{CO}[a] (10^{-3} mol h^{-1} g^{-1} cat.)	NO conv. (%)	N_2O selectivity (%)
300[b]	1.5	5.0	0.58	6.0	63
	2.5	5.0	1.05	6.0	66
	3.5	5.0	1.35	6.0	66
	4.5	5.0	1.81	5.95	66
	4.9	4.9	1.88	7.6	66
	5.0	5.0	1.96	5.9	67
	5.0	5.0	1.96	6.1	58
	5.0	6.0	1.90	6.5	58
	5.0	7.0	1.78	6.1	58
	5.0	8.0	1.75	6.6	57
	5.0	9.0	1.68	5.3	58
120[c]	2.1	4.4	0.44	11.9	86
	3.2	4.5	0.42	10.9	78
	3.4	4.2	0.55	13.1	72
	4.3	4.6	0.53	10.0	71
	5.2	4.5	0.61	9.3	66
	6.6	4.2	0.67	7.8	54
	8.0	4.4	0.74	6.9	54
	3.5	3.9	0.70	10.4	70
	4.3	4.5	0.95	14.6	73
	4.3	5.5	0.89	14.4	79
	4.1	7.3	0.82	13.2	79
	4.2	8.4	0.92	13.7	78

[a] Rate of CO oxidation by reaction with NO calculated from the CO conversion given by Eq. [12].

[b] Space velocity, 120,000 h^{-1}. Rate measurements on an aged catalyst after reaction at 500°C for 16 h.

[c] Space velocity, 25,000 h^{-1}.

between 2.1–8.0 × 10^{-3} atm for P_{NO} and 3.9–8.4 × 10^{-3} atm for P_{CO}, and in the range 1.5–5 × 10^{-3} atm for P_{NO} and 4.9–9 × 10^{-3} atm for P_{CO}, respectively. The apparent orders with respect to NO and CO partial pressures, calculated from the rate values in Table 1, are listed in Table 2. The comparison with the CO order value obtained on Pt–Rh/Al_2O_3 at 300°C shows significant attenuation of the CO-inhibiting effect on the reaction rate after ceria addition. The positive value obtained at 120°C invalidates Eq. [8], which only admits values between −1 and 0. The selectivity on Pt–Rh/Al_2O_3–CeO_2 also differs according to the temperature range conditions (see Table 1). The selectivity for the production of N_2O (S_{N_2O}), calculated at 300°C, is independent of the NO and CO partial pressures, similarly to what was observed on Pt–Rh/Al_2O_3 at the same temperature.Conversely S_{N_2O} continuously decreases with a rise in P_{NO} at 120°C.

TABLE 2

Influence of Ceria Addition on the Apparent Reaction Orders for the CO + NO Reaction over Bimetallic Pt, Rh Catalysts

Catalysts	T (°C)	P_{CO} (10^{-3} atm)	P_{NO} (10^{-3} atm)	m[a]	n[a]
Pt–Rh/Al_2O_3[b]	300	3.0–8.0	1.5–5.7	−0.38	0.40
Pt–Rh/Al_2O_3–CeO_2	300	4.9–9.0	1.5–5.0	−0.27	0.98
Pt–Rh/Al_2O_3–CeO_2	120	3.9–8.4	2.1–8.0	0.16	0.42

[a] $r_{CO} = k P_{CO}^m \times P_{NO}^n$.

[b] See Ref. (13).

3.2. Surface Characterization

3.2.1. X-ray photoelectron spectroscopy observation. Figure 3 shows X-ray photoelectron (XP) spectra of the Ce 3d core level for Pt–Rh/Al_2O_3–CeO_2 directly introduced into the analysis chamber and after *in situ* reduction in H_2 at 425°C. Ce $3d_{5/2}$ and Ce $3d_{3/2}$ photopeaks can be decomposed into five contributions: u_0, u_1, u_2, u_3, and u_4, and v_0, v_1, v_2, v_3, and v_4, respectively (23). However the lowest binding energy contributions, u_0 and v_0, are usually difficult to resolve (23–25). As observed in Fig. 3, only four contributions are distinguishable for each group, which have been assigned in accordance with the literature data. The spectrum recorded before *in situ* thermal treatment (see Fig. 3A) is dominated by the contribution $u_1(v_1)$, $u_3(v_3)$, and $u_4(v_4)$, which mainly characterizes Ce^{4+} species in Pt–Rh/Al_2O_3–CeO_2. As illustrated in Fig. 3B, significant modifications occur after reduction since the most intense signals, $u_1(v_1)$ and $u_2(v_2)$, indicate the predominant formation of Ce^{3+}. The quantitative analysis of XP spectra is summarized in Table 3 and shows surface Rh-enriched catalysts compared to bulk compositions. It is worthwhile to note that a reducing treatment induced surface Ce and Pt enrichment, mainly on Pt–Rh/Al_2O_3–CeO_2, in accordance with the current trends reported in the literature (26).

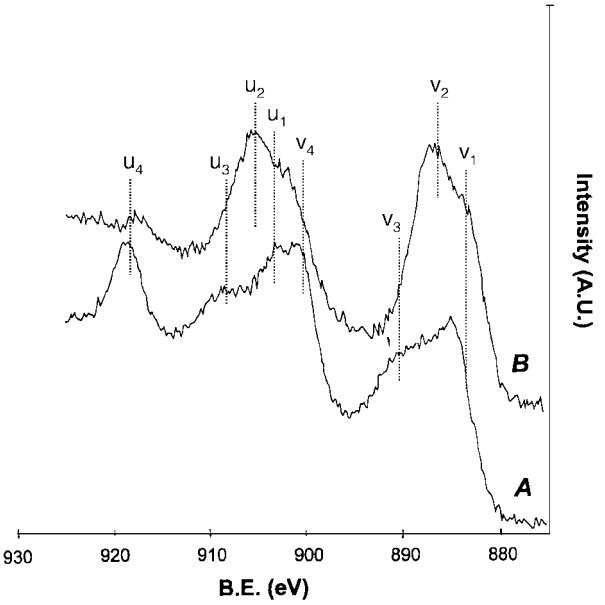

FIG. 3. X-ray photoelectron spectra of Ce 3d core level in Pt–Rh/Al_2O_3–CeO_2 without prior thermal treatment (A) and after reduction in 10 vol% He at 425°C (B).

TABLE 3

Surface Composition of Bimetallic Pt–Rh Supported on γ-Al_2O_3 and after Modification by Ce Addition

Catalyst	Pretreatment	Bulk atm. composition		Surface atm. composition				B.E. (eV)	
		Ce/Ce + Al	Rh/Rh + Pt	Pt/Al	Rh/Al	Ce/Ce + Al	Rh/Rh + Pt	Pt $3d_{3/2}$	Rh $3d_{5/2}$
Pt–Rh/Al_2O_3	Initial		0.27	2.0×10^{-3}	0.8×10^{-3}		0.29	332.4	308
	Reduced[a]			2.3×10^{-3}	0.9×10^{-3}		0.29	332.1	307.6
Pt–Rh/Al_2O_3–12 wt% CeO_2	Initial	3.9×10^{-2}	0.27	2.0×10^{-3}	2.2×10^{-3}	5.7×10^{-2}	0.52	332.9	307.7
	Reduced[a]			4.1×10^{-3}	3.2×10^{-3}	6.7×10^{-2}	0.44	331.4	307.4

[a] After reduction in 10 vol% H_2 in helium at 425°C.

3.2.2. Infrared observations. The FTIR spectra in Figs. 4 and 5 were recorded at room temperature after exposure to 1.3×10^{-2} atm of CO for 1 h on prereduced samples and evacuation under vacuum. The desorption of CO irreversibly adsorbed was further studied between 25 and 300°C. Figure 4a shows IR spectra of CO adsorbed on Pt–Rh/Al_2O_3 mainly characterized by an absorption band at 2060 cm^{-1}; a broad and weaker band at 1840 cm^{-1} is also detected. According to previous assignments, they mainly characterize, respectively, linear and bridge-bonded CO mainly adsorbed on Pt^0 (27–30). The asymmetry of the peak at 2060 cm^{-1} could be due to a minor contribution of the asymmetric stretching mode of gem dicarbonyl species at ~2030 cm^{-1}. An increase in temperature under vacuum activates the desorption of adsorbed CO molecules visualized by a subsequent attenuation of these absorption bands and a shift toward lower frequencies at the same time. Finally, CO on Pt–Rh/Al_2O_3 completely desorbs when the temperature rises to 300°C. Figure 5

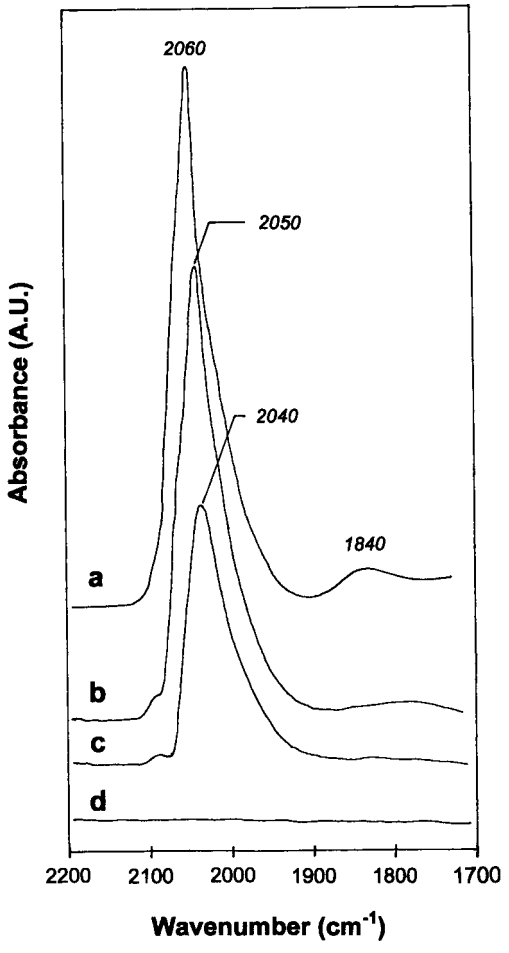

FIG. 4. Infrared spectra of CO adsorbed on prereduced Pt–Rh/Al_2O_3 after desorption under vacuum at various temperatures: 25°C (a); 100°C (b); 200°C (c); and 300°C (d).

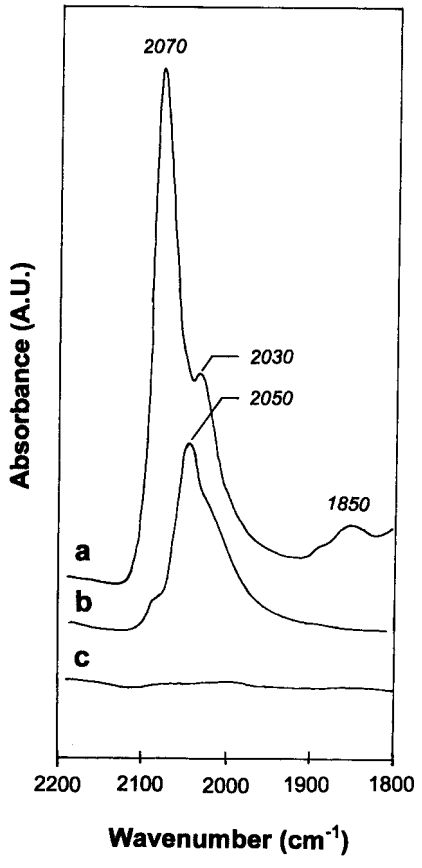

FIG. 5. Infrared spectra of CO adsorbed on prereduced Pt–Rh/Al_2O_3–CeO_2 after desorption under vacuum at various temperatures: 25°C (a); 100°C (b); and 200°C (c).

illustrates changes in the FTIR spectra of CO adsorbed on $Pt–Rh/Al_2O_3–CeO_2$ after desorption at various temperatures using a similar experimental procedure. As previously observed on $Pt–Rh/Al_2O_3$, linear CO species over noble metals still predominate on the ceria-modified catalyst, with the presence of bridge-bonded CO species occurring to a lesser extent. The highest resolution of the IR band at 2030 cm^{-1}, assigned to $Rh^+(CO)_2$ species, is in accordance with the highest surface Rh composition of $Pt–Rh/Al_2O_3–CeO_2$. No significant changes in the overall intensity of absorption bands is distinguishable in comparison with $Pt–Rh/Al_2O_3$. A further increase in temperature leads to similar features previously observed on $Pt–Rh/Al_2O_3$ associated with the desorption of CO. It is interesting that complete desorption of CO on $Pt–Rh/Al_2O_3–CeO_2$ operates at a lower temperature, ~200°C, than that on $Pt–Rh/Al_2O_3$, which indicates weaker CO adsorption on the prereduced $Pt–Rh/Al_2O_3–CeO_2$ catalyst.

4. DISCUSSION

Clearly the kinetic behavior of $Pt–Rh/Al_2O_3–CeO_2$ for the CO + NO reaction is strongly dependent on the temperature-range conditions. As observed, addition of ceria to noble metals lowers the CO-inhibiting effect on the reaction rate at 300°C and decreases the apparent activation energy. Such tendencies are more pronounced at 120°C, with a slight positive value for the CO order, which is inconsistent with Eq. [8], previously established from a mechanism involving only steps on the metals (12, 13). Consequently, this shift to positive values should be related to changes in the reaction mechanism.

The promotor effect of ceria has already been explained (3, 4, 9, 19, 31) by the reactivity of oxygen from ceria, at the vicinity of CO molecules adsorbed on the metal particles at the metal/ceria interface, with subsequent formation of anionic vacancies which are further replenished via the dissociation of NO adsorbed on the metals. The following bifunctional mechanism scheme is usually used for explaining the rate enhancement in the CO + NO reaction. It also involves steps ([13a]–[14b]) on metals previously depicted in the introduction and on ceria.

$$CO_{ads} + O \rightarrow CO_{2g} + V + *, \quad [13a]$$

$$CO_g + O \rightarrow CO_{2g} + V, \quad [13b]$$

$$NO_{ads} + V \rightarrow N_{ads} + O, \quad [14a]$$

$$NO_g + V + * \rightarrow N_{ads} + O, \quad [14b]$$

$$NO_{ads} + N_{ads} \rightarrow N_2O_g + 2*, \quad [4]$$

$$NO_{ads} + N_{ads} \rightarrow N_{2g} + O_{ads} + *, \quad [5]$$

$$N_{ads} + N_{ads} \rightarrow N_{2g} + 2*, \quad [6]$$

where V and O, respectively, stand for an anionic vacancy and a reactive oxygen species from ceria; $*$ is a free adsorption site on the metals; and CO_{ads}, NO_{ads}, and N_{ads} are on a metal site. The direct reaction between gaseous CO and oxygen from ceria seems to be in disagreement with earlier observations. Several workers (3, 4, 9) claimed that the activation of CO by adsorption on the metal is essential to promote the CO + NO reaction. Previous investigations of the CO + NO reaction performed in our laboratory over ceria-promoted catalysts seem also to be in agreement with this statement (20). The consensus on the refilling of the oxygen vacancies in ceria either with NO adsorbed or in the gas phase (steps [14a] and [14b]) seems to be less general. As a matter of fact, Fornasiero *et al.* (3) preferred step [14b], but with no really decisive arguments in our opinion. Since the fundamentals of catalysis is based on the activation of reagents by adsorption, we will assume that NO adsorbed on metals is considerably more reactive than NO in the gas phase and consequently will neglect step [14b]. Recent transient kinetic studies of the CO + NO reaction on $Pt–Rh/\gamma\text{-}Al_2O_3–CeO_2$ (32, 33) have shown that NO can adsorb on ceria but is unable to dissociate, which emphasizes the fact that the adsorption of NO over noble metals is a requisite step for activating its dissociation on anionic vacancies from ceria.

Another tentative explanation for the effect of ceria relies on a possible modification of the adsorptive properties of noble metals in interaction with ceria in accordance with Oh (9), who evidenced strong modifications in NO adsorption and dissociation on Rh in the presence of ceria. Finally he explained the promoting effect of ceria without involving the intermediate formation of oxygen vacancies as active sites for NO dissociation. In a recent study of the CO + NO and CO + N_2O reactions on ceria-modified Pd- and Rh-based catalysts, Holles *et al.* (34) modeled their results by assuming a mechanism involving only noble metals, but they concluded that the presence of electrophilic sites at the interface of ceria/noble metals is crucial in the dissociation of NO. In fact, these earlier investigations assumed the existence of various possible mechanisms which are sometimes difficult to unambiguously discriminate. This is well illustrated by the work of Nibbelke *et al.* (11) on the CO + O_2 reaction on $Pt–Rh/\gamma\text{-}Al_2O_3–CeO_2$, where they showed that a monofunctional mechanism, where the reaction is catalyzed only by noble metals, and a bifunctional one, involving reaction paths between CO adsorbed on the metal and oxygen from ceria at the metal/ceria interface, are equally in agreement with their kinetic results from a statistical point of view.

In the light of these considerations, it seems obvious that ceria can exhibit different effects as a consequence either of modifications in the electronic properties of noble metals, and consequently their adsorption properties, or of the participation of active oxygen species from ceria. Accordingly the monofunctional mechanism depicted in the introduction and the bifunctional one can be equally considered for modeling rate measurements. Consequently, the rate

equation for CO oxidation by NO could be the sum of the rates of both mechanisms.

The rates of steps [3] (r_3) and [9] (r_9) can easily be established as functions of the CO and NO partial pressures. However the rates of NO conversion into N_2 and N_2O (r_{NO}) or of CO oxidation into CO_2 (r_{CO}) in the two mechanisms are not directly related to r_3 and r_{14}. According to the overall transformation of NO and CO (see Eqs. [9] and [10]), the expressions of r_{NO} and r_{CO} are

$$r_{NO} = 2\left(r_{N_2O} + r_{N_2}\right) = 2(r_4 + r_5 + r_6), \qquad [15]$$

and

$$r_{CO} = r_{N_2O} + 2r_{N_2} = r_4 + 2r_5 + 2r_6, \qquad [16]$$

where r_{N_2O} and r_{N_2} are, respectively, the rates of NO transformation into N_2O and N_2 ($r_{N_2O} = r_4$ and $r_{N_2} = r_5 + r_6$). Hence, the rates r_{CO} and r_{NO} can be related to the selectivity for the production of N_2O according to Eq. [17]:

$$S_{N_2O} = \frac{r_{N_2O}}{r_{N_2O} + r_{N_2}} = \frac{r_4}{r_4 + r_5 + r_6}. \qquad [17]$$

In the case of the monofunctional mechanism previously established on Pt–Rh/Al_2O_3, involving only metal sites (steps [1]–[7]), the following equation can be obtained by applying the steady state approximation to adsorbed N atoms:

$$\frac{d\theta_N}{dt} = 0 = r_3 - r_4 - r_5 - 2r_6. \qquad [18]$$

Hence,

$$r_{1NO} = 2r_3 - 2r_6. \qquad [19]$$

Now, considering that at high temperature the synergy effect of ceria is suppressed, it is reasonable to assume that at 300°C the monofuctional mechanism predominates, which is in agreement with the selectivity (S_{N_2O}) independence of P_{NO} and P_{CO} observed at that temperature on Pt–Rh/Al_2O_3–CeO_2 and Pt–Rh/Al_2O_3. Such selectivity behavior implies necessarily that the rate of step [6] is negligible in comparison of that of steps [4] and [5], as already explained (13). Consequently for the mechanism on metals, r_6 can be neglected in Eq. [19], leading to the equation

$$r_{1NO} \cong 2r_3 = 2k_3\theta_{NO}\theta^*, \qquad [20]$$

where θ_i and θ^* are, respectively, coverage for the reactant i and the fraction of vacant metal sites.

If we still assume for Pt–Rh/Al_2O_3–CeO_2 preferential adsorptions of NO and CO, respectively, on Rh and Pt, and that NO dissociates on a nearest-neighbor Pt site, as we have already shown to probably occur on Pt–Rh/Al_2O_3 (13), then θ^* and θ_{CO} represent the fraction of vacant Pt sites or Pt sites covered with adsorbed CO molecules, while θ_{NO} stands for the coverage of NO adsorbed on Rh. θ_{CO} and θ_{NO} can be easily derived:

$$\theta_{CO} = \frac{\lambda_{CO}P_{CO}}{1 + \lambda_{CO}P_{CO}}, \qquad [21]$$

$$\theta_{NO} = \frac{\lambda_{NO}P_{NO}}{1 + \lambda_{NO}P_{NO}}, \qquad [22]$$

and

$$\theta^* = 1 - \theta_{CO} = \frac{1}{1 + \lambda_{CO}P_{CO}}. \qquad [23]$$

Equations [21]–[23] can further be introduced into Eq. [20], which yields Eq. [24]:

$$r_{1NO} = \frac{2k_3\lambda_{NO}P_{NO}}{(1 + \lambda_{CO}P_{CO})(1 + \lambda_{NO}P_{NO})}. \qquad [24]$$

Regarding the rate of CO oxidation via the monofunctional mechanism, Eqs. [15] and [16] can be simplified, considering, as mentioned before, that r_6 is negligible, thus Eq. [25] can be obtained,

$$\frac{r_{1CO}}{r_{1NO}} = \frac{r_4 + 2r_5}{2(r_4 + r_5)} = \frac{k_4\theta_{NO}\theta_N + 2k_5\theta_{NO}\theta_N}{2(k_4\theta_{NO}\theta_N + k_5\theta_{NO}\theta_N)}, \qquad [25]$$

leading to Eq. [26],

$$r_{1CO} = \left[\frac{k_4 + 2k_5}{2(k_4 + k_5)}\right] r_{1NO}, \qquad [26]$$

and finally to Eq. [27],

$$r_{1CO} = \frac{k\lambda_{NO}P_{NO}}{(1 + \lambda_{CO}P_{CO})(1 + \lambda_{NO}P_{NO})}, \qquad [27]$$

with

$$k = k_3\left(\frac{k_4 + 2k_5}{k_4 + k_5}\right). \qquad [28]$$

Regarding the bifunctional mechanism involving active oxygen species from ceria and which is supposed to occur at low temperature, the rate of CO_2 formation is that of step [13],

$$r_{2CO} = k_{13}\theta_{CO}\theta_O, \qquad [29]$$

where θ_O is the fraction of surface oxygen from ceria. As demonstrated in the Appendix, Eq. [30] can be established:

$$r_{2CO} = \frac{k_{13}k_{14}\lambda_{NO}\lambda_{CO}P_{NO}P_{CO}}{k_{14}\lambda_{NO}P_{NO}(1 + \lambda_{CO}P_{CO}) + k_{13}\lambda_{CO}P_{CO}(1 + \lambda_{NO}P_{NO})}. \qquad [30]$$

Consequently the rate of the overall CO_2 production on Pt–Rh/Al_2O_3–CeO_2 is given by Eq. [31]:

$$r_{CO} = \frac{k\lambda_{NO}P_{NO}}{(1+\lambda_{CO}P_{CO})(1+\lambda_{NO}P_{NO})} + \frac{k_{13}k_{14}\lambda_{NO}\lambda_{CO}P_{NO}P_{CO}}{k_{14}\lambda_{NO}P_{NO}(1+\lambda_{CO}P_{CO})+k_{13}\lambda_{CO}P_{CO}(1+\lambda_{NO}P_{NO})}. \quad [31]$$

Such an equation cannot be linearized and, further, be solved using a usual graphic method. Only an optimization method, earlier described (12), using nonlinear regression analysis can be applied for adjusting the rate constant k, k_{13}, and k_{14} and the equilibrium constants of the reactants λ_i. The adjustment routine has been achieved using the solver set up on Excel 5 from Microsoft. It consists of minimizing the square difference between experimental rates, shown in Table 1, and those calculated from Eq. [31].

4.1. Effect of Ce Additive on the Kinetic Behavior of Noble Metals at 120°C

The results obtained from the optimization routine, using the set of rates at 120°C, are reported in Table 4. The value for k, the rate constant related to the dissociation over noble metals, is much smaller than for k_{13} and k_{14}. Consequently, at this temperature the dissociation of NO on the metals is very slow, which leads to the conclusion that a reaction path with the conventional mechanism involving only noble metals is unable to model the CO + NO reaction at 120°C ($r_{1CO} = 2.2 \times 10^{-5}$ mol h^{-1} g^{-1} in comparison with $r_{2CO} = 7.1 \times 10^{-4}$ mol h^{-1} g^{-1} for $P_{NO} = 4 \times 10^{-3}$ atm and $P_{CO} = 4 \times 10^{-3}$ atm), the bifunctional reaction paths [13] and [14] being probably the most representative. Accordingly, at low temperature, the rate equation of CO transformation $r_{CO} \sim r_{2CO}$.

Using rate measurements obtained at various temperatures, as shown in Fig. 1, we have attempted to model the temperature dependency of parameters included in Eq. [31]. It consists of determining the preexponential factors A, A_{13}, A_{14}, and f_i of the rate constant k_{13}, k_{14}, and of the equilibrium constants of the reactants λ_i and the corresponding values for the activation energies (E, E_{13}, and E_{14}) and for the adsorption enthalpies of the reactants $\Delta H_{ads,i}$ in Eqs. [32]–[35]:

$$k = A\exp\left(-\frac{E}{RT}\right), \quad [32]$$

$$k_{13} = A_{13}\exp\left(-\frac{E_{13}}{RT}\right), \quad [33]$$

$$k_{14} = A_{14}\exp\left(-\frac{E_{14}}{RT}\right), \quad [34]$$

$$\lambda_i = f_i\exp\left(-\frac{\Delta H_{ads,i}}{RT}\right). \quad [35]$$

The adjusted values are listed in Table 5. As observed in Fig. 6, they lead to reasonable agreement between experimental and predicted rates using the optimized parameters.

TABLE 4

Optimized Kinetic and Thermodynamic Constants for the CO + NO Reaction at 120°C on Pt–Rh/Al_2O_3–CeO_2

Rate constants of reaction paths involving ceria (mol h^{-1} g^{-1})	
k_{13}	89.5×10^{-3}
k_{14}	1.2×10^{-3}
Rate constant of paths involving the metals (mol h^{-1} g^{-1})	
k	2.7×10^{-4}
Equilibrium adsorption constants (atm^{-1})	
λ_{NO}	353
λ_{CO}	751

TABLE 5

Temperature Dependence on the Kinetic and Thermodynamic Constants for the CO + NO Reaction at 120°C on Pt–Rh/Al_2O_3–CeO_2

	Preexponential factor		Activation energy, E (kJ mol^{-1})	Adsorption enthalpy, $\Delta H_{ads,i}$ (kJ mol^{-1})
	A (mol h^{-1} g^{-1})	f_i (atm^{-1})		
Steps on the metals	1.0×10^{11}		110.2	
Step [13a]	6.1×10^{12}		104.7	
Step [14a]	3.3×10^{3}		48.5	
NO adsorption		4.9×10^{-4}		−44.3
CO adsorption		0.38		−24.9

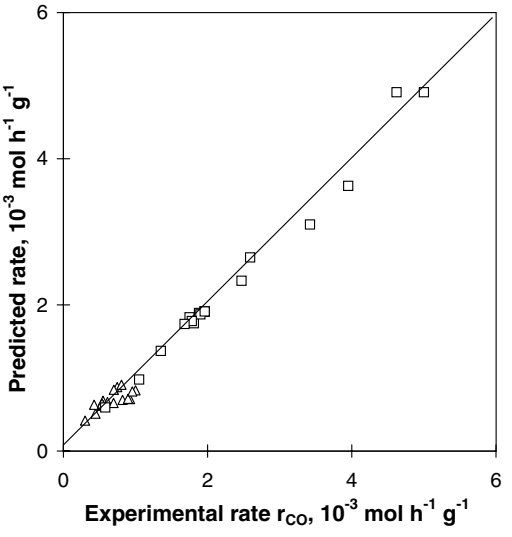

FIG. 6. Correlation between experimental and calculated rates on Pt–Rh/Al_2O_3–CeO_2 in the temperature ranges 110–120°C (△) and 300–330°C (□).

Two major comments arise from the examination of these optimized parameters. First, the energy of activation corresponding to the step of oxygen consumption (step [13a]) is substantially higher than that of the refilling step of anionic vacancies (step [14a]). Consequently at high temperature, the extent of ceria reduction will be high and θ_O very low, which will lower the rate of step [13a]. This is in good agreement with the interpretation of the loss of synergy effect at high temperature by ceria reduction. Second, the values for the adsorption enthalpies of CO and NO are comparable with those calculated on the reference $Pt–Rh/Al_2O_3$ catalyst according to the margin of error (see Table 7). This observation suggests that no significant interaction between ceria and noble metals occurs at low temperature, which could alter their electronic properties (35) and subsequently their adsorption properties.

4.2. Kinetic Behavior of the Aged Pt–Rh/Al_2O_3–CeO_2 at 300°C

Let us remember that steady state kinetic experiments were performed after aging of the reactant mixture at 500°C for 16 h, which could lead to some modifications in its catalytic performances mainly due to deactivation, as indicated by temperature-programmed (TP) experiments, which showed that the beneficial effect of ceria on NO conversion is significantly attenuated for a longer period of time.

As previously mentioned, at 300°C, ceria is probably extensively reduced. At that temperature, the ratio k_{13}/k_{14} would be $\sim 1.4 \times 10^4$, as calculated from the values shown in Table 5 and the reaction paths including ceria should be negligible. Consequently, the transformation of NO would predominantly involve noble metals at 300°C and would obey the classical Langmuir–Hinshelwood mechanism earlier described. It is noteworthy that the selectivity values for the transformation of NO into N_2O (Table 1) are insensitive to changes in the partial pressure of the reactants, mimicking the selectivity behavior of $Pt–Rh/Al_2O_3$ and Rh/Al_2O_3 (13). Such an observation supports the previous conclusion and can probably be related to a preferential adsorption of NO on Rh in $Pt–Rh/Al_2O_3–CeO_2$, since the subsequent dissociation of adsorbed NO molecules yielding chemisorbed N atoms on Rh is consistent with the fact that only steps [4]–[6] are involved in the transformation of NO. The insensitivity of S_{N_2O} to P_{NO} also suggests that the associative desorption of chemisorbed N atoms via step [6] is slow in comparison with the fast steps [4] and [5], as already discussed (13). Consequently, $r_{CO} \sim r_{1CO}$ at 300°C on $Pt–Rh/Al_2O_3–CeO_2$.

The optimized values for k, λ_{CO}, and λ_{NO} are reported in Table 6. Comparison of the parameters k and λ_i with those estimated on the reference $Pt–Rh/Al_2O_3$ at 300°C shows significant differences mainly associated with a sharp decrease in λ_{NO} and to a lesser extent in λ_{CO}, which substantiates a lessening of the CO-inhibiting effect after ceria addition. With regard to the rate constant k (per gram of catalyst), no significant conclusion can be drawn relative to the ceria-induced effect on the rate of NO dissociation since the determination of the metal dispersion is difficult to assess from hydrogen or CO chemisorption on $Pt–Rh/Al_2O_3–CeO_2$ (36, 37). Additionally XPS and infrared spectroscopy of CO adsorption observations underline a surface rhodium composition higher than that of $Pt–Rh/Al_2O_3$. Hence, it is expected that the intrinsic rate constant (per surface Rh atom) varies differently than the specific rate constant (4.73×10^{-3} against 38.5×10^{-3} mol h^{-1} g^{-1}), with Rh being much more active than Pt for the dissociation of NO (38, 39). Both the highest surface Rh composition and the surface modifications, related to sintering reactions (40) which might occur during reaction at 500°C, could also cause changes in the rate of dissociation of NO, which is known to be structure sensitive (41).

TABLE 6

Kinetic and Thermodynamic Constants for the CO + NO Reaction at 300°C on $Pt–Rh/Al_2O_3–CeO_2$

Catalyst	Rate contant, k (mol h^{-1} g^{-1})	Adsorption constant[a] (atm^{-1})	
		λ_{NO}	λ_{CO}
Aged $Pt–Rh$ on $Al_2O_3–CeO_2$	38.5×10^{-3}	12.1	29.9
$Pt–Rh/Al_2O_3$	4.7×10^{-3}	505	122

[a] Noncompetitive adsorption of NO and CO, respectively, on Rh and Pt site.

The lower activation energy of step [14a] relative to step [13a], calculated using rate measurements at low-temperature, and the low value of k_{14}/k_{13} at 300°C indicate extensive reduction of Ce^{4+} into Ce^{3+} during pretreatment at 500 and 300°C. From this explanation it seems obvious that kinetic data obtained at 300°C reflect the influence of reduced ceria, with the subsequent formation of anionic vacancies interacting with noble metals, on the kinetic behavior of $Pt–Rh/Al_2O_3–CeO_2$.

The values of preexponential factors A and f_i (for k and λ_i), the activation energy E corresponding to the rate of NO dissociation on the metal, and $\Delta H_{ads,i}$ are reported in Table 7. Figure 6 shows that a good quality of fit between experimental and predicted rates, using the adjusted parameters shown in Table 7, is obtained. Comparison of these parameters with those previously calculated on $Pt–Rh/Al_2O_3$ (42) shows a significant decrease in the activation energy of NO dissociation and in the adsorption enthalpies of the reactants. The weakening of the CO–Pt and NO–Rh bonds could be due to anionic vacancies interacting with noble metals in $Pt–Rh/Al_2O_3–CeO_2$ and leading to a strong metal-support-type interaction, which usually alters

TABLE 7

Optimised Kinetic and Thermodynamic Parameters for the CO + NO Reaction on Aged Pt–Rh/Al_2O_3–CeO_2

Catalyst	Preexponential factor			Adsorption enthalpy		Activation energy, E^a (kJ mol^{-1})
	A (mol g^{-1} h^{-1})	f_{CO} (atm^{-1})	f_{NO} (atm^{-1})	$\Delta H_{ads,CO}$ (kJ mol^{-1})	$\Delta H_{ads,NO}$ (kJ mol^{-1})	
Aged Pt–Rh on Al_2O_3–CeO_2	1.6×10^9	0.52	2.3×10^{-2}	−19.4	−30.1	117.2
Pt–Rh/Al_2O_3	1.3×10^9	0.86	5.8×10^{-2}	−26.1	−43.8	123.8

[a] Activation energy associated with the rate-limiting step ($NO^* + * \rightarrow N^* + O^*$).

the chemisorptive capacity of noble metals, particularly toward hydrogen adsorption (43). Of course no conclusive statements relative to either the nature and/or the extent of interaction in Pt–Rh/Al_2O_3–CeO_2 can be drawn from examination of our kinetic data at 300°C. Infrared spectroscopic measurements give additional arguments for discussion relative to the difference observed in the strength of the CO–metal bond. Clearly CO is more weakly adsorbed over noble metals on prereduced Pt–Rh/Al_2O_3–CeO_2 than on Pt–Rh/Al_2O_3. These spectroscopic features corroborate our kinetic data, which showed a significant decrease in the adsorption enthalpy of NO and CO on Pt–Rh/Al_2O_3–CeO_2. Such observations are not presently explained and necessitate further investigation. These modifications could be due either to deactivation in the course of the reaction, via an accumulation of isocyanate, which was found to alter the adsorption properties of Pt (44), or to a weakening of the metal–CO bond, as previously proposed by Chafik *et al.* (45) for the CO + NO reaction on Rh/TiO_2. These authors explained their results as the unavailibilty of unoccupied states of Rh metal to form a σ-bond and a subsequent lesser back-donation into the $2\pi^*$ of CO even when Rh exhibits electron-enriched d orbitals.

5. CONCLUSION

The influence of Ce additive on the catalytic performances of three-way bimetallic Pt–Rh/Al_2O_3 in the CO + NO reaction has been investigated. Preliminary TP experiments evidenced a beneficial effect of ceria on the conversion of NO mainly at low temperatures. Above 280°C, Pt–Rh/Al_2O_3–CeO_2 behaves apparently similarly to Pt–Rh/Al_2O_3. An extensive kinetic study at 120 and 300°C, corresponding to temperatures where, respectively, the ceria-induced effect on activity is predominant and suppressed, has been performed in an attempt to explain these results. It was found that a bifunctional mechanism involving reaction of oxygen from ceria with adsorbed CO molecules on the metals, then dissociation of adsorbed NO molecules on anionic vacancies, correctly fits rate measurements at 120°C. At low temperatures, the refilling step [14a] is fast enough to avoid extensive ceria reduction. Consequently Ce^{4+} probably predominates at the surface. The low steady state surface concentration of anionic vacancies probably prevents strong interaction between ceria and noble metals, preserving adsorption properties similar to those characteristic of Pt–Rh/Al_2O_3. On the other hand, drastic changes in kinetics operates at 300°C, when probably only noble metals catalyze the CO + NO reaction. It was also found that at high temperatures ceria is probably extensively reduced into Ce^{3+}, with the subsequent formation of anionic vacancies in the vicinity of metal particles, and that the strong interaction generated with noble metals alters their electronic properties, subsequently modifying their adsorption properties mainly by weakening the CO– and NO–metal bond.

APPENDIX

The rate of CO_2 production according to a bifunctional mechanism (as shown earlier) is

$$r_{2CO} = k_{13}\theta_{CO}\theta_O. \quad [29]$$

θ_O can be obtained by applying the steady state approximation to oxygen species from ceria,

$$\frac{d\theta_O}{dt} = 0 = k_{14}\theta_{NO}\theta_V - k_{13}\theta_{CO}\theta_O, \quad [36]$$

with

$$1 = \theta_V + \theta_O, \quad [37]$$

where θ_V is the fraction of oxygen vacancies on ceria. Thus,

$$\theta_O = \frac{k_{14}\theta_{NO}}{k_{14}\theta_{NO} + k_{13}\theta_{CO}}. \quad [38]$$

Consequently,

$$r_{2CO} = \frac{k_{13}k_{14}\theta_{CO}\theta_{NO}}{k_{14}\theta_{NO} + k_{13}\theta_{CO}}. \quad [39]$$

Accounting for preferential adsorptions of CO and NO, respectively, on Pt and Rh, θ_{NO} and θ_{CO} can be replaced by

Eqs. [21] and [22], leading ultimately to Eq. [30]:

$$r_{2CO} = \frac{k_{13}k_{14}\lambda_{NO}\lambda_{CO}P_{NO}P_{CO}}{k_{14}\lambda_{NO}P_{NO}(1+\lambda_{CO}P_{CO}) + k_{13}\lambda_{CO}P_{CO}(1+\lambda_{NO}P_{NO})}. \quad [30]$$

ACKNOWLEDGMENTS

We gratefully acknowledge the Institut Francais du Petrole and the CNRS, which initiated this work through a research group, "Groupement de Recherche Pot Catalytique," and Mr. J. Billy, who conducted infrared measurements.

REFERENCES

1. Taylor, K. C., *Catal. Rev.–Sci. Eng.* **35**, 457 (1993).
2. Schelef, M., and Graham, G. W., *Catal. Rev.–Sci. Eng.* **36**, 433 (1994).
3. Fornasiero, P., Ranga Rao, G., Kaspar, J., L'Eratio, F., and Graziani, M., *J. Catal.* **175**, 269 (1998).
4. Ranga Rao, G., Fornasiero, P., Di Monte, R., Kaspar, J., Vlaic, G., Balducci, G., Meriani, S., Gubitosa, G., Cremona, A., and Graziani, M., *J. Catal.* **162**, 1 (1996); Ranga Rao, G., Kaspar, J., Di Monte, R., Meriani, S., Gubitosa, G., and Graziani, M., *Catal. Lett.* **24**, 107 (1996).
5. Schmieg, S. J., and Belton, D. N., *Appl. Catal.* **58**, 131 (1979).
6. Sanchez, M. G., and Gazquez, J.-L., *J. Catal.* **104**, 120 (1987).
7. Summer, J. C., and Ausen, S. A., *J. Catal.* **58**, 131 (1979).
8. Kim, G., *Ind. Eng. Chem. Prod. Res. Dev.* **21**, 267 (1982).
9. Oh, S. H., *J. Catal.* **124**, 477 (1990).
10. Loof, P., Kasemo, B., Anderson, S., and Frestad, A., *J. Catal.* **130**, 181 (1991).
11. Nibbelke, R. H., Campman, M. A. J., Hoebink, J. H. B. J., and Marin, G., *J. Catal.* **171**, 358 (1997).
12. Granger, P., Dathy, C., Lecomte, J.-J., Leclercq, L., Prigent, M., Mabilon, G., and Leclercq, G., *J. Catal.* **173**, 304 (1998).
13. Granger, P., Dathy, C., Lecomte, J.-J., Leclercq, L., and Leclercq, G., *J. Catal.* **175**, 194 (1998).
14. Lecomte, J. J., Granger, P., Leclercq, L., Lamonier, J.-F., and Aboukais, A., *Colloid Surf. A* **158**, 241 (1999).
15. Leclercq, G., Dathy, C., Mabilon, G., and Leclercq, L., *in* "Catalysis and Automotive Pollution Control II" (A. Crucq, Ed.), p. 181. Elsevier, Amsterdam, 1991.
16. Shwartz, J. M., and Schmidt, L. D., *J. Catal.* **148**, 22 (1994).
17. Chojnacki, T., Krause, K., and Schmidt, L. D., *J. Catal.* **128**, 161 (1991).
18. Golunski, S. E., Hatcher, H. A., Rajaram, R. R., and Truex, T. J., *Appl. Catal. B* **5/4**, 367 (1995).
19. Harrison, B., Diwell, A. F., and Hallett, C., *Platinum Met. Rev.* **32**, 73 (1988).
20. Granger, P., Lamonier, J.-F., Sergent, N., Aboukais, A., Leclercq, L., and Leclercq, G., *Top. Catal.* **16/17**, 89 (2001).
21. Zafiris, G. S., and Gorte, R. J., *J. Catal.* **143**, 86 (1993).
22. Serre, C., Garin, F., Belot, G., and Maire, G., *J. Catal.* **141**, 9 (1993).
23. Romeo, M., Bak, K., El Fallah, J., Lenormand, F., and Hilaire, L., *Surf. Int. Anal.* **2**, 508 (1993).
24. Lenormand, F., Hilaire, L., Kili, K., Krill, G., and Maire, G., *J. Phys. Chem.* **92**, 2561 (1998).
25. Ramarason, E., Tempere, J.-F., Guilleux, M. F., Vergand, F., Roulet, H., and Dufour, G., *J. Chem. Soc., Faraday Trans.* **88**, 1211 (1992).
26. Nieuwenhuys, B. E., *Adv. Catal.* **44**, 259 (1999).
27. Unpublished results obtained at the Institut de Recherches sur la Catalyse.
28. Yang, A. C., and Garland, C. W., *J. Phys. Chem.* **61**, 1504 (1957).
29. Yates, D. J. C., Murel, L. L., and Prestridge, E. B., *J. Catal.* **84**, 41 (1979).
30. Solymosi, P., *J. Phys. Chem.* **89**, 4789 (1985).
31. Oh, S. H., and Eickel, C. C., *J. Catal.* **112**, 543 (1988).
32. Harmsen, J. M. A., Hoebink, J. H. B. J., and Shouten, J. C., *Catal. Lett.* **71**, 81 (2001).
33. Harmsen, J. M. A., Hoebink, J. H. B. J., and Shouten, J. C., *Stud. Surf. Sci. Catal.* **133**, 349 (2001).
34. Holles, J. H., Switzer, M. A., and Davis, R. J., *J. Catal.* **190**, 247 (2000).
35. Martinez-Arias, A., Soria, J., and Conesa, J. C., *J. Catal.* **168**, 364 (1997).
36. Trovarelli, A., Dolcetti, G., de Leitenburg, C., Kaspar, J., Finetti, P., and Santoni, A., *J. Chem. Soc., Faraday Trans.* **88**, 1311 (1992).
37. Cordatos, H., and Gorte, R. J., *J. Catal.* **159**, 112 (1996).
38. Gorte, R. J., and Schmidt, L. D., *Surf. Sci.* **109**, 367 (1990).
39. Wickam, D. T., Banse, B. A., and Koel, B. E., *Surf. Sci.* **243**, 83 (1991).
40. Krause, K. R., and Schmidt, L. D., *J. Catal.* **140**, 424 (1993).
41. Peden, C. H. F., Belton, D. N., and Schmieg, S. J., *J. Catal.* **155**, 204 (1995).
42. Granger, P., Lecomte, J.-J., Leclercq, L., and Leclercq, G., *Appl. Catal.* **208** (2001).
43. Tauster, S. J., Fung, S. C., and Garten, R. L., *J. Am. Chem. Soc.* **100**, 170 (1978).
44. Lorimer, D., and Bell, A. T., *J. Catal.* **59**, 223 (1979).
45. Chafik, T., Kondarides, D. I., and Verykios, *J. Catal.* **190**, 446 (2000).